Applied Catalysis A: General 490 (2015) 117–127

Contents lists available at ScienceDirect

Applied Catalysis A: General

journal homepage: www.elsevier.com/locate/apcata

Preparation of selective $ZnCl_2$/alumina catalysts for methyl chloride synthesis: Influence of pH, precursor and zinc loading

Sabrina A. Schmidt[a,*], Markus Peurla[b], Narendra Kumar[a], Kari Eränen[a], Dmitry Yu. Murzin[a], Tapio Salmi[a]

[a] Åbo Akademi University, Department of Chemical Engineering, Process Chemistry Centre, Laboratory of Industrial Chemistry and Reaction Engineering, FI-20500 Åbo/Turku, Finland

[b] University of Turku, Department of Cell Biology and Anatomy, Laboratory of Electron Microscopy, FI-20520 Turku, Finland

ARTICLE INFO

Article history:
Received 13 May 2014
Received in revised form 4 November 2014
Accepted 6 November 2014
Available online 14 November 2014

Keywords:
Methyl chloride
Chloromethane
Heterogeneous catalyst
Alumina
Zinc chloride

ABSTRACT

Zinc-modified alumina catalysts for methyl chloride synthesis were prepared with varying zinc loadings: from 2.4 to 21.1 wt%. The influence of the zinc loading, zinc precursor and the pH of the impregnation on the physico-chemical properties of the catalyst, and on the catalyst activity and selectivity for methyl chloride (MeCl) synthesis was investigated. The prepared catalysts were thoroughly characterized by FTIR, TEM, physisorption and EDX. On the alumina surface, both molecular and bulk zinc species are created upon zinc loading. The surface area of the catalyst decreases steadily with zinc loading. Bulk zinc species dominate on the catalyst starting at a zinc loading of 9.4 wt% and the amount of Lewis acid sites (LAS) decreases. A shift in the acid site type takes place upon zinc modification. Sites assigned to stronger LAS are eliminated while zinc-based weaker acid sites started to predominate. The shift in acidity increases the selectivity and activity of methyl chloride synthesis, which was demonstrated in a series of experiments in a laboratory-scale fixed bed reactor.

1. Introduction

Methyl chloride is a chemical intermediate that is used for the synthesis of butyl rubber, silicones, methyl cellulose and as a general methylation agent. It can be produced by gas-phase hydrochlorination of methanol over a Lewis acidic heterogeneous catalyst at atmospheric pressure and temperatures around 300 °C. Dimethyl ether is formed as a side-product, but can react in a consecutive reaction with HCl to form methyl chloride. The reaction scheme is shown below:

$$CH_3OH + HCl \leftrightarrow CH_3Cl + H_2O \quad (I)$$

$$2CH_3OH \leftrightarrow (CH_3)_2O + H_2O \quad (II)$$

$$(CH_3)_2O + HCl \leftrightarrow CH_3Cl + CH_3OH \quad (III)$$

Industrially neat or zinc-modified alumina are used as catalysts. Neat alumina is an inexpensive catalyst but it is less active and requires higher reaction temperatures [1,2]. Zinc-modified zeolites have been studied, but alumina-based catalyst, both, neat and zinc-modified, have shown a superior stability [3]. Thus, zinc-modified alumina is an attractive catalyst for the intensified production of methyl chloride and was first proposed as a catalyst for methyl chloride synthesis by Svetlanov et al. in 1967 [4]. By addition of Zn^{2+} additional Lewis acid sites (LAS) are created which act as active sites [3]. The addition of zinc lowers the adsorption enthalpy of methanol [4]. $ZnCl_2$/alumina can also be used as a catalyst for other types of reactions e.g. olefin metathesis in combination with CH_3ReO_3 [5–7] and hydrochlorination of ethene [8]. Thus, a deeper understanding of the catalyst properties is desirable. In-depth characterization of zinc modified alumina catalysts was carried out to identify active sites and understand the physico-chemical and catalytic properties. Different active species have been proposed, such as amorphous zinc chloride [8] and a molecular zinc species on the alumina surface [5]. A common observation is that upon zinc modification of alumina, terminal hydroxyl groups are eliminated which suggests that zinc reacts directly with the alumina surface [5–7]. This is also supported by the observation of a chlorine-to-zinc ratio lower than two when the catalyst was calcined at higher temperatures [5].

This study aims to provide detailed characterization of zinc-modified alumina with varying zinc loadings and connect the catalyst properties with the catalytic activity in methyl chloride synthesis. The acid properties, the nature of the active sites and the chemical nature of the zinc species on the surface were

* Corresponding author. Tel.: +358 469064572.
E-mail address: sschmidt@abo.fi (S.A. Schmidt).

http://dx.doi.org/10.1016/j.apcata.2014.11.008
0926-860X/

characterized and related to the catalytic activity and selectivity, which are gradually changing with zinc loading.

2. Experimental

2.1. Catalyst preparation

The zinc chloride modified catalysts were prepared by wet impregnation. Four grams of ball-milled and sieved alumina (UOP Versal VGL-25 (<32 μm)) were added to a solution of the required amount of $ZnCl_2$ (Fluka, ≥98%) or $Zn(NO_3)_2$ (hexahydrate, Fluka, ≥99.0%) in 200 mL distilled water. The zinc loading in wt% corresponds to the relative mass of Zn^{2+} ions on the alumina. The pH of the impregnation solutions is given in Table 1. To investigate the influence of pH of the impregnation solution the pH was adjusted by adding HCl or NH_3 respectively. The solution was rotated for 24 h at 65 °C, and subsequently, the water was evaporated at 70–80 °C under vacuum. The catalyst was calcined in a step calcination procedure: 40 min at 200 °C and subsequently 3 h at 400 °C applying a heating rate of 3 °C/min.

2.2. Catalyst characterization

2.2.1. Nitrogen-physisorption

The specific surface area and pore volume of the catalysts were determined by nitrogen-physisorption (Carlo Erba Sorptometer 1900). The surface area and pore volume were calculated using the BET and the Dollimore–Heal method respectively. Prior to the measurements, the samples were outgassed under vacuum for 3 h at 150 °C.

2.2.2. Fourier transform infrared spectroscopy (FTIR)

The amount of Lewis and Brønsted acid sites on the catalysts was quantified by Fourier transform infrared spectroscopy (FTIR) using pyridine as the probe molecule (ATI Mattson Infinity Series). The catalyst was pressed to a wafer (ca. 10 mg) and placed in the measurement cell. Prior to pyridine adsorption, the sample was outgassed under vacuum (0.08 mbar) for 1 h at 450 °C and background spectra were recorded at 100 °C. Pyridine was adsorbed for 30–90 min at 100 °C and spectra were recorded at 100 °C after heating to 250, 350 and 450 °C respectively. The Lewis acidity was determined from the adsorption band at 1455 cm^{-1} and the Brønsted acidity from the adsorption band at 1545 cm^{-1} according to Emeis [9]. FTIR spectra of the OH vibrational modes were recorded at 100 °C after outgassing under vacuum (0.08 mbar) for 1 h at 450 °C.

2.2.3. Energy dispersive X-ray microanalysis (EDX)

The zinc and chlorine contents of the catalysts were investigated by energy-dispersive X-ray microanalysis (EDX) (Zeiss Leo Gemini 1530). The catalysts used for the EDX analysis were pressed to wafers. Due to the high density of the wafers, the quantification was more precise and charging of the zeolite samples during the measurement was reduced.

Table 1
pH of the support/$ZnCl_2$ dispersion for impregnation.

Catalyst	pH
Alumina 2.4 wt% Zn ($ZnCl_2$)	5.6
Alumina 4.5 wt% Zn ($ZnCl_2$)	5.6
Alumina 4.5 wt% Zn ($ZnCl_2$)	4.0
Alumina 4.5 wt% Zn ($ZnCl_2$)	8.5
Alumina 4.5 wt% Zn ($ZnCl_2$)	10.6
Alumina 4.5 wt% Zn ($Zn(NO_3)_2$)	6.0
Alumina 8 wt% Zn ($ZnCl_2$)	5.7
Alumina 14 wt% Zn ($ZnCl_2$)	5.6
Alumina 19 wt% Zn ($ZnCl_2$)	5.4
Alumina 22 wt% Zn ($ZnCl_2$)	5.4
Alumina 25 wt% Zn ($ZnCl_2$)	5.3

2.2.4. Inductively coupled plasma-optical atomic emission spectroscopy (ICP-OES)

To confirm the results obtained by EDX, inductively coupled plasma atomic emission spectroscopy (ICP-OES) was performed for one sample. Approximately 40 mg was weighed into a Teflon bomb and digested in a microwave oven with 3 mL H_2SO_4 (96%) and 3 mL HNO_3 (65%). The sample was diluted to 500 mL prior to the ICP-OES analysis.

2.2.5. pH dependent zeta potential

The neat alumina powder (ball-milled and sieved, <32 μm) was dispersed in deionized water (2 mg/L). The pH dependent zeta potential was determined using the Zetasizer Nano and the MPT-2 automatic titrator by Malvern Instruments. The titrations were performed at 25 °C and aqueous NaOH and HCl were used as titrants. Zeta potential was calculated from the electrophoretic mobility using the Smoluchowski model.

2.2.6. Transmission electron microscopy (TEM)

The zinc modification on the catalyst surface was determined by transmission electron microscopy (TEM) (JEOL JEM-1400Plus) using imaging and electron diffraction functions. The samples were prepared either from powder or from aqueous solution. The powder samples were prepared by blowing powder on the TEM grid with the use of a pipette. The aqueous samples were prepared by loading a 1.5 mL microtube with 0.1 mL of catalyst powder. The tube was then filled up to 1 mL with purified water. The dispersion was homogenized by shaking and exposing to 5 min of ultrasound. Large catalyst particles that would not be transparent to the electron beam were separated by centrifugation for 30 s at 1000 rpm. The remaining solution was diluted 1:100, transferred on the TEM grid and dried in vacuum.

For imaging an accelerating voltage of 120 kV was used, and for electron diffraction either 80 or 120 kV. To obtain the *d*-spacing from the electron diffraction patterns, a reference pattern (aluminum foil) was recorded at identical microscope settings. In some samples, a layer of graphene oxide was coated on the TEM grid prior to sample deposition and used as internal calibration standard. The recorded diffraction patterns were analyzed using the software Diffraction Ring Profiler 1.7, which was developed for phase identification in complex microstructures [10].

2.2.6.1. Sample stability. No changes in the sample morphology were observed during investigation of the materials with an electron beam strength of 80 or 120 kV. Thus, the samples were considered to be stable. In the case of electron diffraction, a decrease in diffractogram quality was observed after investigating a sample area for more than a few minutes. The decreased stability is due to a very small sample area exposed to the beam during electron diffraction. Thus for recording of electron diffractograms, the analysis time was minimized so that no sample decay occurred.

2.2.7. X-ray powder diffraction (XRD)

The catalyst crystal structure was determined by X-ray diffraction (XRD) with a Philips X'Pert Pro MPD using monochromatic Cu-K_α radiation. The measured 2θ range was 3.0–75.0° with a step size of 0.04° and a measurement time of 2.0 s per step.

2.3. Methyl chloride synthesis

The reaction was performed in a quartz-made tubular reactor with an inner diameter of 1 cm. 0.05 g of catalyst were loaded into the reactor as a fixed bed between quartz sand and quartz wool. The reactor was equipped with a thermocouple positioned close to the catalytic bed to determine the reaction temperature. The reaction temperature was 210 °C for catalyst screening and 300 °C for catalyst stability tests. The flow rates 10 mL/min He/HCl (AGA, 20.000%), 10 mL/min He and 0.0034 mL/min MeOH (J.T. Baker, HPLC gradient grade) (volumetric flow rates at room temperature). These flow rates gave the stoichiometric HCl:MeOH ratio 1:1 and a helium content of 83% to prevent corrosion. The gas flow was controlled by mass flow controllers (Bronkhorst EL-flow). The liquid methanol was pumped using an HPLC pump (Shimadzu LC-20AD) and evaporated in the heated lines. All the lines and equipment from the methanol inlet to the GC were isolated and heated by electrical heating wires to 96 °C. To guarantee homogeneous methanol evaporation, a helium flow was used. After the reactor, a neutralization bottle (106 °C) filled with calcium oxide (Fischer, general-purpose grade) was installed to remove HCl and water from the product gas. In this way, the corrosion problem was minimized, since water/HCl injections into the GC were prevented. Samples were withdrawn with a heated gas-tight syringe (100 °C) through a septum in the sampling section. Prior to the reactor outlet, a washing bottle filled with a volume based 2:6:2 mixture of water/methanol/ethanol amine (Sigma–Aldrich, ≥98%) at room temperature was placed to strip methyl chloride from the reaction product gas. Swagelok stainless steel lines and valves were used in the equipment. All conversions and selectivities reported were obtained from steady-state experiments. Several samples were withdrawn over at least 200 min to observe catalyst stability and guarantee that the reactor operates at a steady state. Selected experiments were repeated to ensure the reproducibility of the results. The standard deviation of the methanol conversion was lower than 6% and for the selectivity lower than 1% in all experiments. The main error is attributed to the GC analysis and integration of the GC spectra.

The gaseous reaction products obtained were manually injected to the GC. The gas chromatographic analysis of the samples was carried out using an Agilent 6890N GC equipped with an FI detector and an HP-Plot/U Column (30 m, I.D. 0.530 mm, film thickness: 20 μm, T = 110 °C). The system was calibrated for methyl chloride, dimethyl ether and methanol using mixtures of known concentrations. The peaks of all products were calibrated with respect to the methanol peak. The concentration of the separate components were thus calculated using the obtained response factors, the methanol/component peak ratio and the initial methanol flow. The carbon balances are consequently 100% closed.

2.4. Calculation of methanol conversion and methyl chloride selectivity

The methanol conversion and the methyl chloride selectivity were calculated as follows (no products were present in the feed): $X_{MeOH} = (c_{0MeOH} - c_{MeOH})/c_{0MeOH}$ and $S_{MeCl} = c_{MeCl}/(c_{MeCl} + 2c_{DME})$.

3. Results and discussion

3.1. Influence of zinc loading

Zn/alumina catalysts were prepared with nominal Zn loadings from 2.5 to 25 wt% using $ZnCl_2$ as precursor. The content of Zn in wt% as well as the Cl/Zn and Al/Zn ratios determined by EDX are given in Table 2. For all catalysts, the Cl/Zn ratio is significantly lower than two, indicating that chlorine was removed from the catalyst during calcination and released as HCl. With an increasing zinc loading the Cl/Zn ratio was lowered, from 0.78 at 2.4 wt% Zn to 0.31 at a nominal zinc loading of 25 wt%. This indicates that most of the zinc is not present as $ZnCl_2$ on the surface but reacts with the alumina surface or forms separate particles of an oxygen-containing zinc species as ZnO or a zinc chloride hydroxide. Furthermore, zinc chloride could be transferred as a molecular zinc species on the surface, forming e.g. Al—O—Zn—Cl as described by Tovar et al. [5]. The nature of zinc on the catalyst surface is further discussed in the following sections.

The surface areas and pore volumes of neat and zinc-modified aluminas were determined (Table 3). Upon modification with zinc, the surface area and the pore volume are steadily lowered with increasing zinc loading due to pore blocking by bulk zinc species or eventually also due to alumina hydrolysis during impregnation. Hydrolysis of alumina during preparations in aqueous solutions has been reported in the literature [11,12].

The acidity of the neat and zinc-modified aluminas was measured by FTIR spectroscopy using pyridine as the probe molecule. The strength of the acid sites is classified upon the temperature that pyridine desorbs from the catalyst, i.e. desorption between 250 and 350 °C for weak acid sites, 350 and 450 °C for medium acid sites. Strong acid sites retain pyridine at 450 °C. Both neat and zinc-modified aluminas are Lewis acidic and no Brønsted acid sites are present in the catalyst. The acidity profiles of the aluminas are given in Table 3. Upon zinc modification with 2.4 wt% zinc, the share of medium strength acid sites is slightly increased, while upon a further increase of zinc loading, the percentage of weak acid sites increases. The total amount of Lewis acid sites increases upon zinc modification and goes through a maximum at a loading of 5.0 wt%. The decrease in the number of acid sites at higher loadings can be explained by the lowering of total surface area.

3.2. Characterization by FTIR spectroscopy, X-ray powder diffraction (XRD) and TEM analysis

3.2.1. FTIR spectroscopy of OH-stretching region and pyridine adsorbed on the catalyst

To get a more detailed picture of the alumina surface modification by zinc, the OH-stretching region of neat and zinc-modified alumina was studied as well as the vibrational modes of pyridine adsorbed on the catalyst. The surface hydroxyl groups of transitional aluminas have been extensively studied in the literature using IR spectroscopy and quantum chemical calculations in order to understand its catalytic properties [13–15]. Furthermore, the adsorption of pyridine on the Lewis acid sites of alumina has been studied intensively [16–18]. Although numerous investigations have been carried out in this field, the precise assignment of the vibrational bands to a specific surface site is not unequivocally established. The field has recently been reviewed by Busca [19] and the interpretation of the observed vibrational modes in the following discussion is based on this review. As observed by Liu and Truitt [18] and further described by Lundie et al. [16] Lewis acid sites on alumina have neighboring OH groups that have specific vibrational modes. Lewis acid sites with a specific strength can be correlated to a surface hydroxyl mode with a specific wavenumber. Thus, observed OH vibrational modes can serve as an indirect indicator for Lewis acidity of alumina. The association of surface hydroxyl groups with their neighboring Lewis acid sites is based on the work of Lundie et al. [16].

3.2.2. Pyridine vibrational modes

The IR-spectra of pyridine absorbed on neat and zinc-modified alumina are shown in Fig. 1. It is clearly visible that neat alumina has mainly two kinds of acid sites, characterized by two

Table 2
Zinc content in wt% of prepared catalysts determined by XPS and EDX.

Catalyst [nominal zinc loading] precursor $ZnCl_2$	Zn EDX [wt%]	ICP-OES [wt%]	Cl/Zn atomic ratio	Al/Zn
Alumina 2.4 wt% Zn	2.4	n.d.	0.78	46.4
Alumina 4.5 wt% Zn	5.0	n.d.	0.56	21.7
Alumina 8 wt% Zn	9.4	n.d.	0.63	10.6
Alumina 14 wt% Zn	14.9	n.d.	0.49	6.2
Alumina 19 wt% Zn	19.5	18	0.40	4.4
Alumina 22 wt% Zn	20.4	n.d.	0.43	4.2
Alumina 25 wt% Zn	21.1	n.d.	0.31	4

Table 3
Surface area [m^2/g], pore volume [cm^3/g] and Lewis acidity of the prepared catalysts.

Catalyst [actual zinc loading] precursor $ZnCl_2$	Surface area [m^2/g]	Pore volume [cm^3/g]	Lewis acid sites [μmol/g]			
			Total	Weak%	Medium%	Strong%
Neat alumina	270	1.30	107	68	29	3
Alumina 2.4 wt% Zn	248	1.00	137	64	36	0
Alumina 5.0 wt% Zn	236	0.94	147	68	24	7
Alumina 9.4 wt% Zn	209	0.86	141	74	24	1
Alumina 14.9 wt% Zn	207	0.62	119	84	15	1
Alumina 19.5 wt% Zn	182	0.56	123	89	11	0
Alumina 20.4 wt% Zn	162	0.64	101	88	12	0
Alumina 21.1 wt% Zn	154	0.67	106	86	14	0

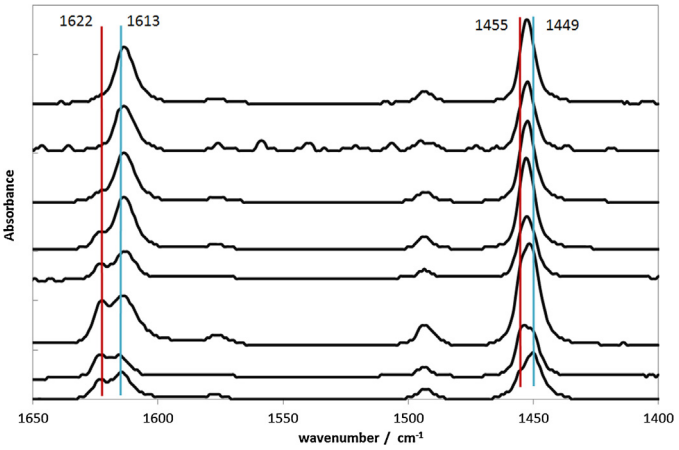

Fig. 1. FTIR spectra of pyridine adsorbed on neat and zinc-modified aluminas. From top to bottom, zinc content: 21.1 wt%, 20.4 wt%, 19.5 wt%, 14.9 wt%, 9.4 wt%, 5.0 wt%, 2.4 wt%, and neat alumina. Spectra recorded at 100 °C after outgassing at 450 °C, subsequent pyridine adsorption and outgassing at 250 °C.

peaks (1455 and 1449 cm^{-1}) for the pyridine 19b vibrational mode and two corresponding peaks for the pyridine 8a mode (1622 and 1613 cm^{-1}) [20]. According to literature, the bands at 1622 and 1455 cm^{-1} correspond to the stronger Lewis acid sites, probably three- and four-coordinated aluminum atoms while the bands at 1613 and 1449 cm^{-1} correspond to weaker acid sites, probably based on octahedrally coordinated alumina. As observed by temperature dependent desorption of pyridine, there are virtually no strong Lewis acid sites on alumina (Table 3). Thus, the bands at 1622 and 1455 cm^{-1} are assigned to the medium LAS as defined by temperature programmed pyridine adsorption.

The vanishing of stronger LAS (1622 and 1455 cm^{-1}) with increasing zinc loading as observed in Fig. 1 suggests that $ZnCl_2$ predominantly interacts with the medium-strong Lewis acid sites on alumina. A possible scheme of this interaction is given in Fig. 3. Concurrently, the share of the peaks at 1613 and 1445 cm^{-1} increases and they slightly shift in wavenumbers, i.e. to 1612 and 1452 cm^{-1} for 21.1 wt% zinc. This indicates the formation of a zinc-based Lewis acid site.

3.2.3. OH-vibrational modes

It has to be noted that an outgassing temperature of 500 °C was used by Busca's review [19] and most of the cited reference within. In this paper an outgassing temperature of 450 °C was used due to technical issues. However, we recorded a spectrum of alumina outgassed at 500 °C not showing any significant changes compared to a somewhat lower outgassing temperature of 450 °C. Furthermore, Morterra and Magnacca [13], Wischert et al. [21] as well as Liu and Truitt [18] reported no significant shifts in peak positions upon variation of the outgassing temperature. The FTIR spectra of the hydroxyl groups observed for neat alumina and for alumina with different zinc loadings are shown in Fig. 2(a). Three distinct vibrational bands were observed, i.e. at 3730, 3685 and 3570 cm^{-1}. These bands are commonly assigned to bridging or triple bridging OH groups, although the band at 3730 cm^{-1} was assigned by Busca [22] to terminal OH groups on octahedrally coordinated aluminum atoms. Interestingly, the bands assigned to terminal OH groups, or, according to Busca [22], terminal OH groups on tetrahedrally coordinated aluminum, are not visible in the spectrum. The terminal OH vibrational modes are located at wavenumbers of 3785–3800 cm^{-1} and 3760–3780 cm^{-1}. These bands are weaker than the bands at a lower wavenumber and their strength depends furthermore on the kind of alumina used [19]. Thus, a reason for the absence of the modes can be the nature of the alumina and the resolution of the spectra. A higher vacuum during outgassing can improve the quality, but could not be reached with the available equipment.

The change in hydroxyl-group population on the alumina surface can be followed clearly by analyzing the difference spectra of the zinc modified aluminas and the neat alumina as shown in Fig. 2(b). With increasing zinc loading the hydroxyl groups with a vibrational mode at 3730 cm^{-1} are strongly decreasing and a less pronounced decrease can be observed for the OH-groups with the vibrational mode at 3685 cm^{-1}. The OH-groups at 3570 cm^{-1} are however not affected. Furthermore, an increase of intensity at 3440 cm^{-1} in the difference spectra can be observed. This band increases with increasing zinc loading and can be assigned to OH groups coordinated to zinc [23]. In summary, the terminal OH groups assigned to higher coordinated alumina and react predominantly with zinc chloride, the bridging OH-groups (3685 cm^{-1}) are less reactive. The higher reactivity of terminal compared to bridging OH groups has furthermore been made by Tovar et al. [5] and Pillai et al. [6,7].

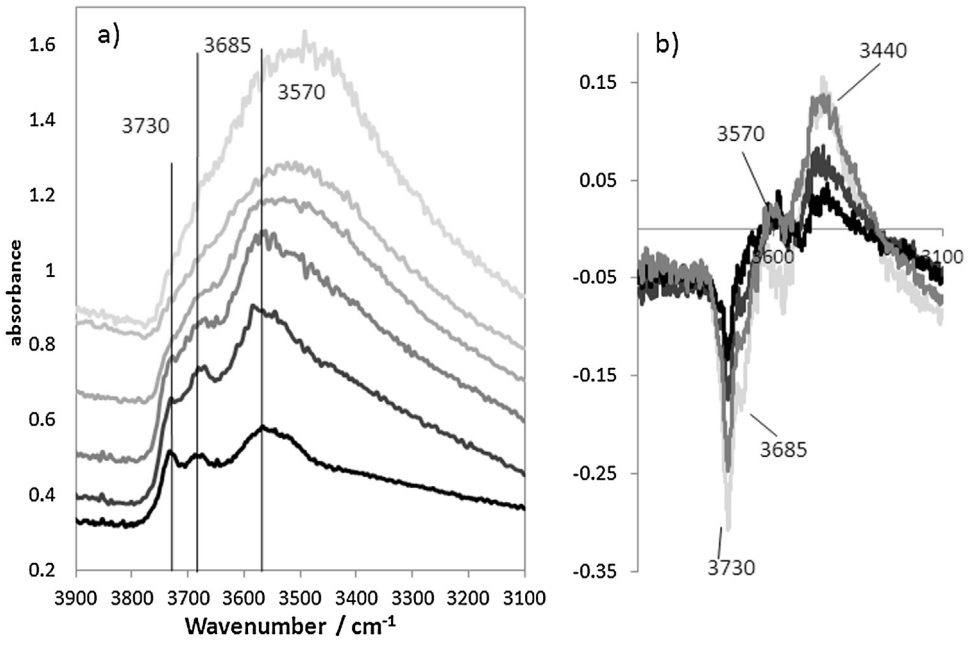

Fig. 2. (a) FTIR spectra of the OH-stretching region of neat and zinc-modified aluminas. From top to bottom, zinc content: 21.1 wt%, 14.9 wt%, 9.4 wt%, 5.0 wt%, 2.4 wt% and neat. Spectra recorded at 100 °C after outgassing at 450 °C for 1 h. (b) Difference spectra of zinc-modified aluminas with respect to the neat alumina. Zinc content: −2.5 wt%, −5 wt%, −9.4 wt% and −50 wt%.

According to Lundie et al. [16] the OH-groups with the vibrational mode at 3730 cm^{-1} can be associated with the medium-weak LAS as observed by pyridine adsorption. Furthermore, the mode at 3685 cm^{-1} can be assigned to the weak Lewis acid sites as observed by pyridine adsorption. The decrease of intensity of these vibrational modes can be correlated with the observed decrease of the pyridine signals assigned to the higher strength LAS (Fig. 1) and attributed to the interaction of the medium LAS with zinc chloride. In case of the weaker acid sites correlated to the OH-group signal at 3685 cm^{-1}, no decrease of the corresponding pyridine vibrational mode can be observed as is overlaps with the vibrational mode of pyridine absorbed on a zinc based active site (1612 cm^{-1}). It has to be remarked that the strongest Lewis acid sites are not associated with a hydroxyl groups according to Lundie et al. [16] and thus cannot be observed in the FTIR spectra.

Starting from a zinc loading of 9.4 wt%, the three OH vibrational bands are perturbed and the band at 3440 cm^{-1} does not increase in intensity anymore. A nearly complete coverage of the alumina surface by zinc species can be assumed. This coincides with the visibility of zinc particles in TEM, i.e. an increased coverage of the alumina surface with bulk Zn(Cl,OH). The TEM results are discussed in the following section.

A reaction scheme of zinc chloride with terminal and bridging OH groups was proposed by Tovar et al. [5] based on IR, NMR and EXAFS analysis of zinc chloride modified alumina. In Fig. 3 this reaction scheme is shown and the above described changes in vibrational modes upon zinc modification are correlated with the involved species in the scheme. The proposed reaction scheme describes well the changes in OH and pyridine vibrational modes upon modification of alumina with zinc chloride observed in the present work.

3.2.4. XRD and TEM analysis

In Fig. 4 XRD pattern of neat alumina, 14.9 wt% and 19.5 wt% $ZnCl_2$/alumina are displayed. The patterns of the zinc-modified aluminas are slightly more defined, but no additional crystalline material besides γ-alumina could be detected in the $ZnCl_2$ modified catalysts using XRD.

This indicates that bulk zinc species as $ZnCl_2$ on alumina are highly amorphous or only a small crystalline fraction is present on the material. In a previous study [3], it was shown that zinc on the alumina surface is present exclusively as Zn^{2+}. To get a deeper understanding of the composition of the zinc-modified catalysts, they were investigated by transmission electron microscopy (TEM), using both imaging and electron diffraction functions. This allows the simultaneous visual and structural analysis of the material, if necessary on selected areas of the samples only a few μm^2 in size.

Samples for TEM analysis were prepared in two ways, from dry catalyst powder and from an aqueous solution. The two methods are described in detail in the experimental section. For the samples prepared from dry powder, no particles could be observed in the TEM images and the material looked identical to the neat support up to the highest loading of 21.1 wt%, which corresponds to a $ZnCl_2$ loading of 51 wt%. The following crystalline phases were detected in dry prepared samples: γ-alumina, $ZnAl_2O_4$ and traces (not statistically relevant) of AlClO. No zinc chloride was detected. The electron diffraction patterns of γ-alumina and $ZnAl_2O_4$ are shown in Fig. 5. Although the diffraction patterns of γ-alumina and the spinel phase of $ZnAl_2O_4$ are almost identical [24,25], diffraction patterns with a strong line at a d-spacing of 1.6 Å characteristic for the spinel phase was only observed in certain diffraction patterns on the zinc-modified catalysts. Thus, it is suggested that the spinel is formed to a small extent upon calcination of $ZnCl_2$ on alumina. Together with the observation of traces of AlClO, it confirms that zinc reacts directly with the support. Nevertheless, the most abundant diffraction pattern is γ-alumina, even at high zinc loadings of 21.1 wt% zinc. This indicates that zinc chloride is present on the catalyst in an amorphous form. However, it was not visible in the TEM images prepared from dry powder.

Preparation of the sample from an aqueous solution has the advantage, that larger catalyst particles can be separated by centrifugation therefore a large number of small catalyst particles transparent to the electron beam are transferred onto the grid. In case of $ZnCl_2$ modified alumina, zinc chloride present on alumina is dissolved in water. As during sample preparation a concentrated dispersion of alumina is prepared and a fraction of larger particles

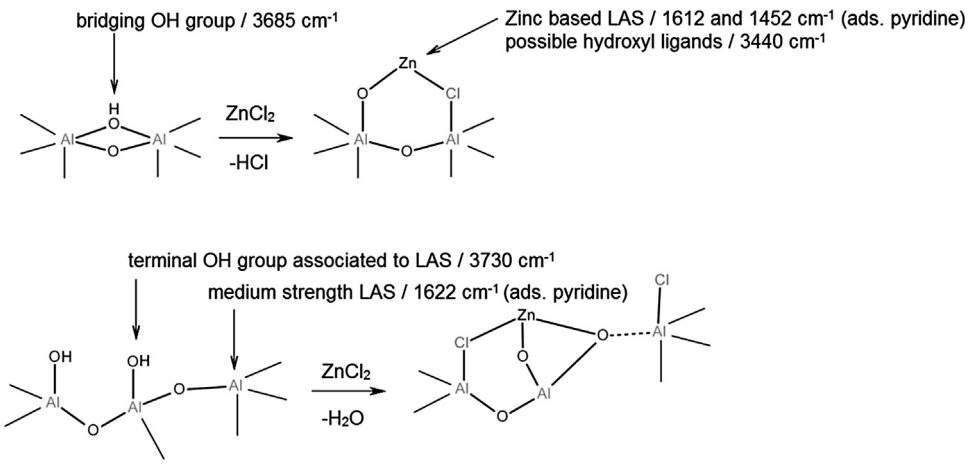

Fig. 3. Reaction of zinc chloride with surface OH-groups adapted from Tovar et al. [5] and correlation with observed vibrational modes.

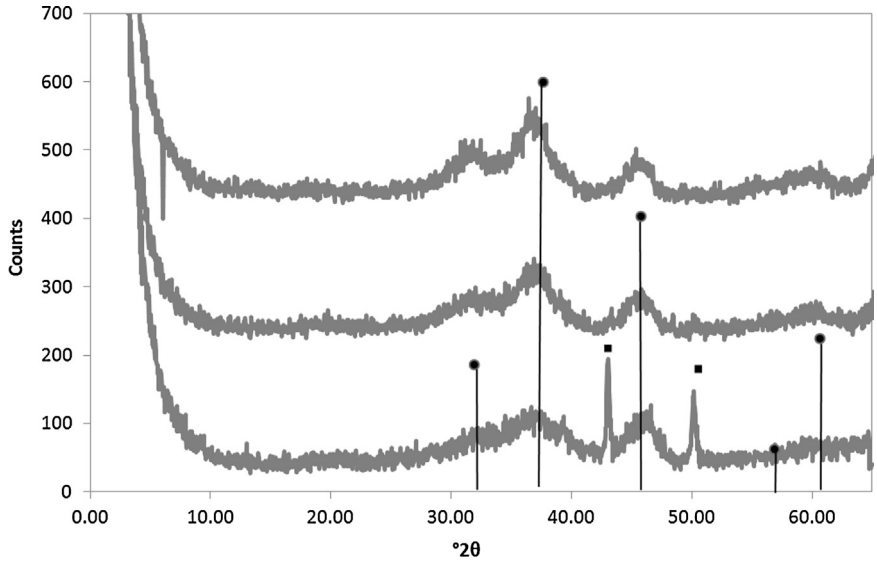

Fig. 4. XRD patterns of (from bottom to top) neat alumina, 14.9 wt% $ZnCl_2$/alumina and 19.5 wt% $ZnCl_2$/alumina. (●) Reference peaks of γ-Al_2O_3, horizontal lines represent relative intensities of reference pattern. (■) Peaks originating from copper sample holder.

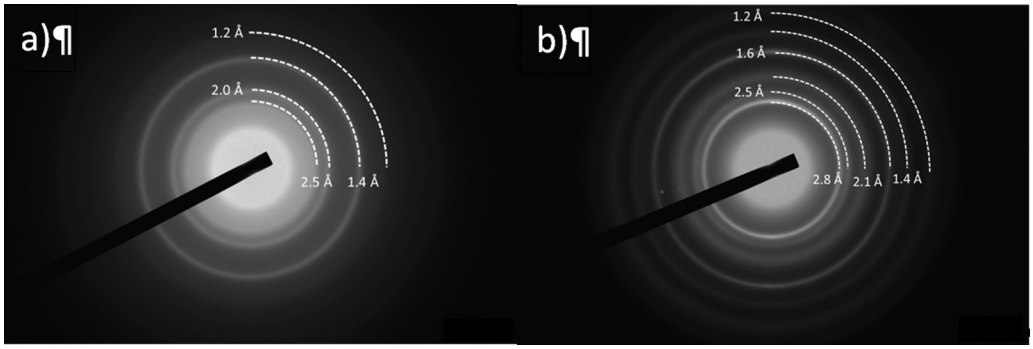

Fig. 5. Electron diffraction pattern for (a) γ-alumina obtained from neat alumina and (b) $ZnAl_2O_4$ obtained from zinc-modified alumina.

removed by centrifugation, dissolved $ZnCl_2$ is enriched in the sample transferred to the grid. As a result, zinc chloride particles are visible on the alumina support starting from a loading of 9.4 wt% (Fig. 6).

The zinc chloride particles are evidently not crystalline, since no electron diffraction pattern could be observed. In two places needle shaped crystals were found and identified as γ-$ZnCl_2$ and traces of Simonkolleite (zinc chloride hydroxide monohydrate) were observed. These two structures were not found in statistically relevant amounts and are described here as supporting information as they are the only zinc species that can be analyzed as they are crystalline. The largest part of $ZnCl_2$ is visible as amorphous particles. The fact that zinc chloride particles are not visible in the dry sample can be explained by formation of a thin layer of zinc

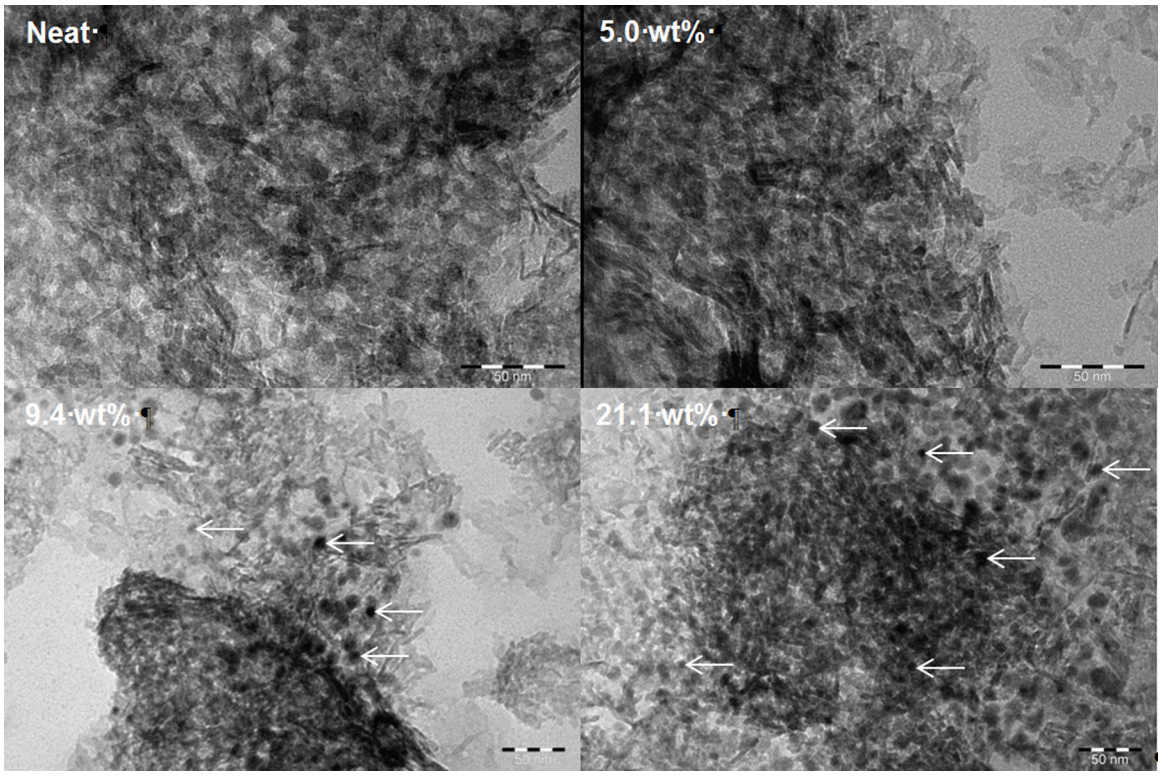

Fig. 6. TEM micrographs of neat and zinc-modified alumina prepared from aqueous solution. Scale bar: 50 nm. The arrows point toward selected zinc particles for illustration.

chloride on the alumina surface that is not visible in the TEM pictures. However, a significant change from 5.0 to 9.4 wt%, i.e. from no visible particles to a large number suggests a possibility that until a loading of 9.4 wt% the zinc mainly reacts with alumina. Molecular zinc surface sites as described in the previous section as well as observed by Trenton et al. [5] and Arndt et al. [26] are formed along with small amounts of $ZnAl_2O_4$.

3.3. *Influence of zinc loading and catalyst acidity on activity and selectivity in methyl chloride synthesis*

The efficiency of the neat and zinc-modified catalysts in the methyl chloride synthesis was compared. Fig. 7 shows that both the methanol conversion and the methyl chloride selectivity increase with zinc loading. The most significant increase of conversion and selectivity was observed upon the first introduction of zinc. With a further increase of zinc loading the methanol conversion increases steadily with zinc loading, while the selectivity does not improve further after a zinc loading of 9.4 wt%.

The activity can be related to the number and strength of the Lewis acid sites as shown in Fig. 8.

When plotting the methanol conversion against the number of Lewis acid sites, it is evident that the activity decreases with an increasing number of acid sites and increases with zinc loading (Fig. 9(a)). Furthermore, with increasing zinc loading, the share of weak acid sites and the methanol conversion increases (Fig. 9(b)). Therefore, it can be concluded that not a higher number or the strength, but rather the nature of the Lewis acid sites determines the catalyst activity. In accordance, the conversion obtained with neat alumina at a comparable number of acid sites is significantly lower as it contains merely weakly active sites originating from alumina. The experimental data show that with an increase of the zinc loading, a shift toward more active and weaker LAS takes place. This correlates with the changes in the vibrational modes of pyridine on alumina and the alumina's surface hydroxyl groups as discussed in Section 3.2.

The selectivity to methyl chloride increases with the share of weak LAS on the catalyst surface until a ratio of weak LAS to total LAS of 0.75 is reached at loading of 9.4 wt% as seen in Fig. 9. In methyl chloride synthesis, the selectivity to methyl chloride increases with conversion due to the formation of methyl chloride from the intermediate product dimethyl ether. To illustrate the higher selectivity of the zinc modified alumina catalysts over a larger range of conversions, the dependence of the methyl chloride selectivity on the methanol conversion is shown in Fig. 9(b). The data is adapted from a previous study of our group [27]. The reaction temperature at which the data was recorded was 280–340 °C, while the reaction temperature in this study was 210 °C. However, it was shown that the correlation of conversion and selectivity is not temperature dependent, so that they can be used for comparison. As expected the recorded conversion and selectivity for neat alumina at 210 °C thus corresponds to the data recorded in [27] at 280 °C. In the case of zinc-modified alumina however, the selectivity at a given conversion is significantly higher.

As the selectivity is constant after a loading of 9.4 wt% is reached, it can be assumed that at this point the zinc-based sites most dominate over the non-selective LAS originating from alumina. Although the share of weak acid sites is still increasing at higher loadings, the selectivity remains stable. This is reflected in the FTIR spectra of the surface hydroxyl groups and pyridine adsorbed on alumina. The observation that the selectivity toward MeCl increases until a zinc loading of 9.4 wt% can be attributed to the point where the share of stronger acid sites (1622 and 1455 cm^{-1}) is compensated by the weaker acid sites that are shifted in wavenumbers, 1612 and 1452 cm^{-1} instead of 1613 and 1449 for pure alumina (Fig. 1).

The formation of molecular zinc species is thought to be more important for methyl chloride synthesis as the major increase in conversion and selectivity is achieved at loadings up to 9.4 wt%, where mainly molecular zinc species are formed. At higher

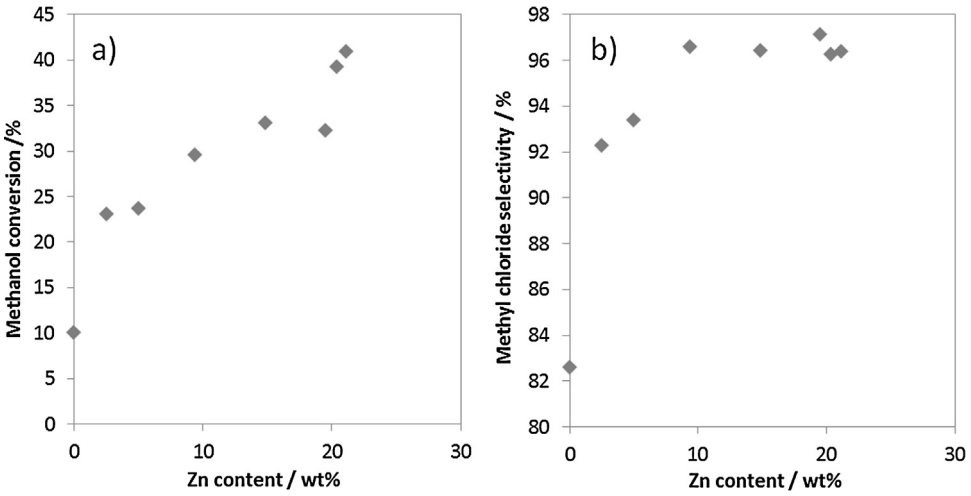

Fig. 7. Influence of zinc content (wt%) on (a) activity and (b) selectivity of methyl chloride.

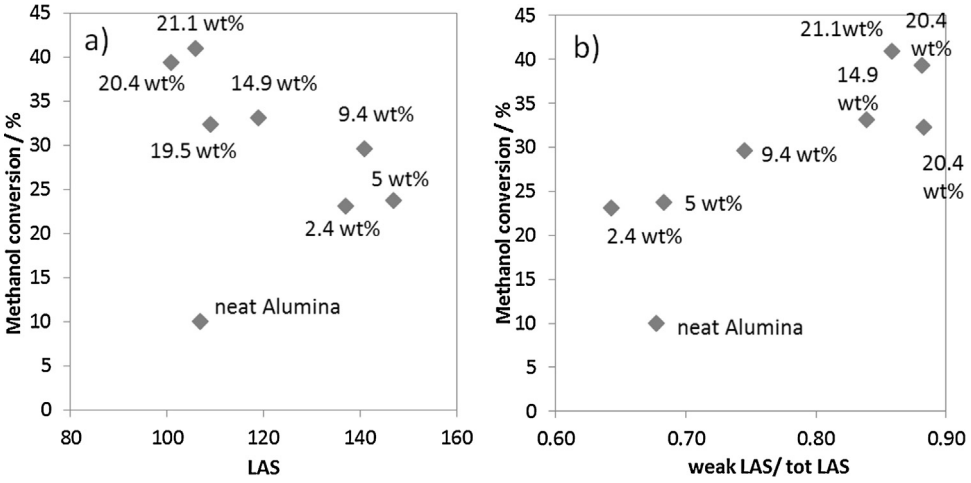

Fig. 8. Influence of (a) Lewis acidity and (b) acid strength on activity in methyl chloride synthesis for neat and zinc-modified catalysts.

loadings, i.e. upon dominant formation of bulk species only minor improvement of catalyst performance could be observed. In conclusion, significantly more active and less strong acid sites created upon zinc modification are resulting in higher selectivity ad activity with an optimum zinc loading of 9.4 wt%.

3.4. Influence of pH and precursor

Zinc-modified alumina with a nominal loading of 5.0 wt% was prepared by wet impregnation with varying pH of the impregnation solution. Furthermore, the influence of the precursor, $ZnCl_2$

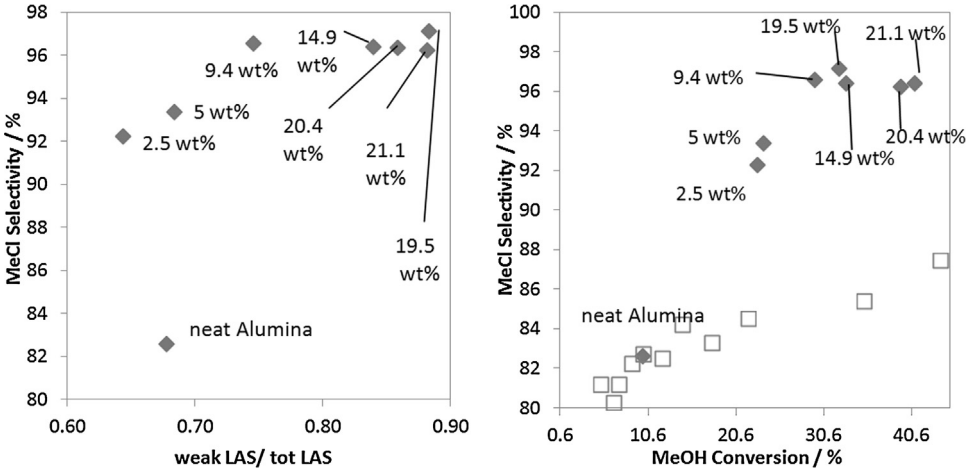

Fig. 9. (a) Influence of acid strength on methyl chloride selectivity for neat and zinc-modified catalysts. (b) Dependence of MeCl selectivity on methanol conversion. Filled symbols: data from the present paper, empty symbols: data from previous experiments for neat alumina illustration published in [40].

Table 4
Specific surface area [m^2/g], pore volume [cm^3/g] and Lewis acidity of catalysts before and after impregnation with $ZnCl_2$/$Zn(NO_3)_2$.

	Surface area [m^2/g]	Pore volume [cm^3/g]	Lewis acid sites [μmol/g]				Zn [wt%]	Cl/Zn atomic ratio
			Total	Weak%	Medium%	Strong%		
Neat alumina	270	1.30	107	68	29	3	–	–
Alumina 4.5 wt% Zn ($ZnCl_2$) pH 4	250	1.02	201	65	27	9	5.4	0.71
Alumina 4.5 wt% Zn ($ZnCl_2$) pH 5.6	236	0.94	147	68	24	7	5.0	0.56
Alumina 4.5 wt% Zn ($ZnCl_2$) pH 8.5	265	1.15	165	65	24	12	5.4	0.69
Alumina 4.5 wt% Zn ($ZnCl_2$) pH 10.6	268	0.97	161	59	30	11	5.2	0.73
Alumina 4.5 wt% Zn ($Zn(NO_3)_2$) pH 6	234	1.00	132	70	19	12	4.6	–

pH 4: |-Al-OH_2^+ / |-Al-O^+ + Zn^{2+}(aq), $ZnCl^+$(aq), $ZnCl_2$(aq) $ZnCl_3^-$ (aq)
zeta potential : 29 mV

pH 5.6: |-Al-OH_2^+ / |-Al-O + Zn^{2+}(aq), $ZnCl^+$(aq), $ZnCl_2$(aq) $ZnCl_3^-$ (aq)
zeta potential: 27 mV

pH 8.5: |-Al-OH + Zn^{2+}(aq), $ZnOHCl_2^-$ (aq) and $Zn_5OH_2Cl_3 \cdot H_2O$ (s)
zeta potential: 0 mV

pH 10.6: |-Al-O^- + $Zn(OH)_3Cl^{2-}$ (aq) and $Zn_5OH_2Cl_3 \cdot H_2O$ (s)
zeta potential: -20 mV

Scheme 1. Schematic representation of the alumina surface and the zinc species in solution dependent on the pH of the impregnation solution.

or $Zn(NO_3)_2$, was investigated. Aqueous solutions of zinc chloride and alumina are complex systems and several pH-dependent factors can influence the final catalyst during the impregnation procedure [28]: surface charge of alumina, species of zinc in the aqueous solution and hydrolysis of alumina. In aqueous solution at ambient temperature alumina is partially hydrolyzed forming small amounts of bayerite, β-$Al(OH)_3$, on its surface [12,29,30]. The formation of bayerite is expected to increase at elevated temperatures as during the impregnation procedure. The surface area was reported to increase with the hydrolysis time of alumina [31] and the solubility of alumina increases with both, increased and decreased pH and increasing temperature. The hydrolysis of alumina is expected to modify mainly the surface area and pore volume of the final catalyst, the formed bayerite is transformed to alumina during the calcination of the catalyst after the impregnation. The zeta potential and the point of zero charge of the used alumina were measured. The pzc was at pH 8.5, which corresponds to previous data for γ-alumina reported in literature [32,33]. Scheme 1 gives an overview on the surface charge of the used γ-alumina and the main zinc species expected in the solution for the different pH [34–38]:

Upon impregnation with zinc, the number of LAS on alumina increases by 30–100% depending on the pH of the impregnation solution, while the total amount of zinc present of the catalysts is similar for all pH (Table 4). The acid strength profile is comparable for all neat and zinc-modified aluminas. From the expected speciation, an increased zinc adsorption leading to an increased amount of acid sites during the impregnation should be observed at pH 4 and pH 5.6, where a mainly positively charged alumina surface and a large fraction of negatively charged $ZnCl_3^-$ (aq) ions are present. However, only at pH 4 an increased number of acid sites compared to the other pH can be observed, although the zeta potential of the alumina is nearly identical at pH 4 and 5.6 (Scheme 1). A reason can be that the concentration of $ZnCl_3^-$ (aq) increases with the Cl^- concentration in the solution. As HCl was added to adjust the pH to four, a higher concentration of negatively charged $ZnCl_3^-$ (aq) might be present in this case. Furthermore, a higher degree of dehydration of the alumina surface can lead to a higher reactivity of the surface. In case of an impregnation solution pH of 8.5 the positively charged Zn^{2+} (aq) is the dominating zinc species in solution. It is expected to react more efficiently with the non-charged alumina surface and a higher amount of acid sites was expected compared to pH 10.6, where a negatively charged alumina surface meets negatively charged zinc hydroxychloride. Nevertheless, both catalysts have a nearly identical acidity. Furthermore, the cases where the alumina surface and the predominant zinc ions in the solution have the same charge, pH 5.6 and pH 10.6, the amount of acid sites created is actually higher in case of pH 10.6. As after zinc adsorption the water is evaporated and remaining zinc is deposited on the catalyst, the effect of pH might be negligible. Furthermore, the point of zero charge is a net value, which still allows local variation of the surface charge. The formation of molecular zinc species by reaction with the Lewis acid sites of alumina (see Section 3.3) can be assumed to take part to a comparable extent at any pH. In conclusion, the pH did not significantly influence the amount of acid sites created on the catalyst, with the exception of the catalyst prepared at pH 4.

In addition to differences in the acidity of the catalysts, significant changes in the surface area were observed. The catalysts prepared without any adjustment of the impregnation solution pH [pH 5.6, $ZnCl_2$ and pH 6, $Zn(NO_3)_2$] have a slightly lower surface area than the neat alumina and the other zinc-modified aluminas, it decreased from 270 m^2/g for neat alumina to about 235 m^2/g. In case of catalysts prepared from a basic solution the surface area is not significantly lowered and for the catalyst prepared from acidified solution, the surface area was diminished to 250 m^2/g. Generally, the reduction of the surface area is caused by pore blockage by bulk zinc species and alumina hydrolysis. However, in case of the pH modified solutions, the surface area is not as severely lowered, as the increased or decreased pH leads to a stronger hydrolysis of alumina resulting in an increase in surface area, as described in [31]. The pore volume was lowered slightly in all cases.

The precursor type used for the zinc modification, i.e. $ZnCl_2$ or $Zn(NO_3)_2$, did not significantly influence the catalyst performance in methyl chloride synthesis (Fig. 10). The reason for the similar activity is the reaction of the catalyst with the gaseous HCl, leading to chlorination of the alumina support as shown below [39,40].

$$Al{-}OH + HCl \rightarrow Al{-}Cl + H_2O$$

Furthermore, $Zn(NO_3)_2$ or ZnO, formed from the nitrate during calcination, can react with HCl to form $ZnCl_2$ which has been reported by Conte et al. [8]. These results in the catalyst being almost identical to alumina modified directly with $ZnCl_2$. This is also supported by the observation that spent Zn/alumina catalysts has a strongly increased Zn/Cl content of 2.52 [3].

3.5. Catalyst stability

All catalysts were tested for 200–300 min at 210 °C and showed no deactivation during this time. The most efficient catalysts with respect to conversion, selectivity and zinc loading were 5 wt% Zn/alumina (pH 5.6) and 9.4 wt% Zn/alumina. Their stability was tested at an elevated temperature of 300 °C for at least 1200 min. For comparison, time-on-stream behavior of neat alumina [41] is

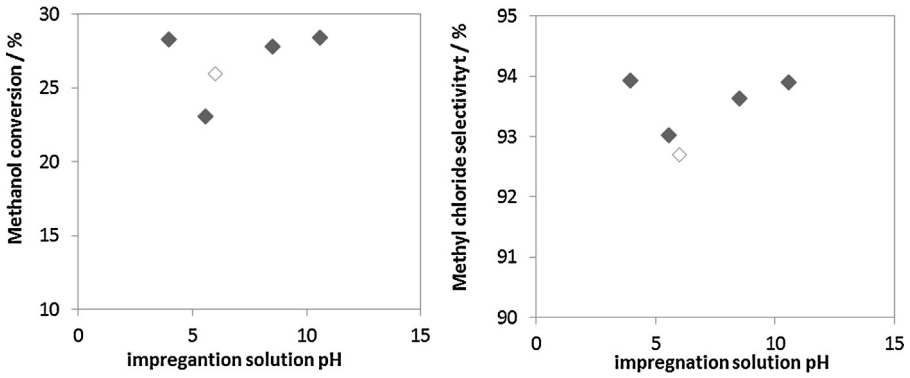

Fig. 10. Methanol conversion and methyl chloride selectivity for catalysts dependent on the impregnation solution pH. $ZnCl_2$ as zinc precursor: blue marks (filled symbols), $Zn(NO_3)_2$ precursor: green marks (empty symbol). (For interpretation of the references to color in this figure legend, the reader is referred to the web version of this article.)

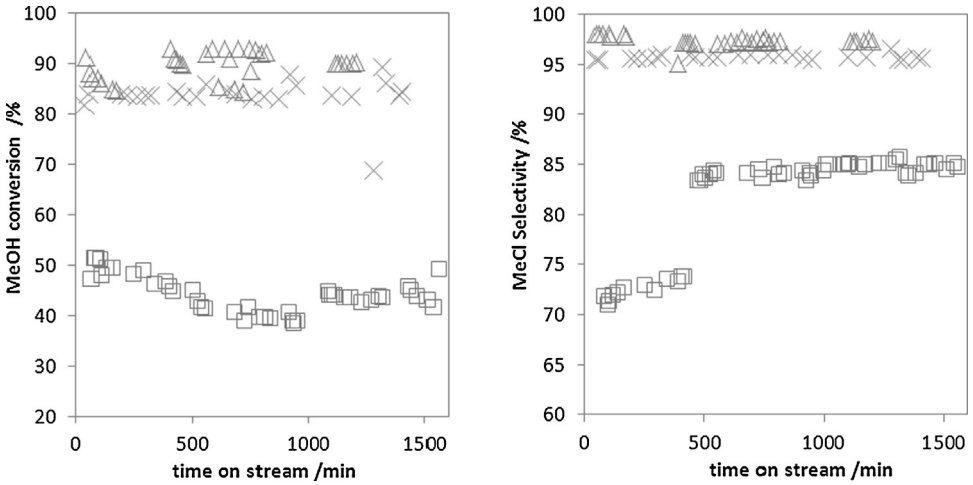

Fig. 11. Methanol conversion and methyl chloride selectivity vs. time on stream for (□) neat alumina ($T = 300°$, adapted from [41]) (×) 5 wt% Zn/alumina (△) 9.4 wt% Zn/alumina.

also shown. The results are displayed in Fig. 11. All catalysts are stable and show no decline of conversion or selectivity. At elevated temperature, high conversion and selectivity can be reached with the zinc-modified catalysts. The alumina with a zinc loading of 9.4 wt% gives the highest conversion (90%) and selectivity (97%). Higher conversion can be obtained by increasing catalyst mass or residence time.

4. Conclusions

Neat and zinc-modified γ-alumina catalysts with different zinc loadings were prepared for methanol hydrochlorination to methyl chloride and thoroughly characterized. The introduction of zinc chloride on alumina significantly increased the activity and selectivity in methyl chloride synthesis. The activity increased steadily with the zinc loading while the selectivity to methyl chloride increased until a loading of 9.4 wt% and remains stable upon further increase of zinc loading. The increase of activity and selectivity in methyl chloride synthesis was correlated with changes in the acid site profile of the catalyst. Upon first introduction of zinc, additional active sites are created, while simultaneously active sites on alumina with a lower selectivity are replaced with more selective and active zinc-based active sites, leading to a higher activity and selectivity. Starting with a loading of 9.4 wt%, the total number of Lewis acid sites decreased. Analysis of the acid properties showed that the neat γ-alumina has two kinds of acid sites characterized by two distinct pyridine vibrational modes. The mode assigned to the stronger acid sites disappears gradually with an increasing zinc loading. In accordance with previous studies, the zinc reacted with terminal OH groups and to a lesser extent with bridging OH-groups to form molecular zinc species. Furthermore, the pyridine modes corresponding to weaker acid sites shift slightly in wavenumber, which is accredited to the formation of zinc based Lewis acid sites. It was concluded, that the decrease of strong acid sites, assigned to tetrahedral coordinated alumina without associated OH-groups, and medium-strong Lewis acid sites, assigned to terminal OH groups bound to a neighboring alumina of the acid site, and the simultaneous increase of zinc based Lewis acid sites are responsible for the shift in acidity, selectivity and activity. Until a loading of 9.4 wt%, mainly molecular zinc species are formed on the alumina surface. At higher loadings bulk zinc species are formed. Using electron diffraction amorphous $ZnCl_2$ and $ZnAl_2O_4$ could be defined as dominant bulk zinc species. Zinc chloride does not form particles on the alumina surface but a thin amorphous layer. In contrast to zinc loading, the pH of the impregnation solution or the nature of the zinc precursor, $ZnCl_2$ or $Zn(NO_3)_2$ did not significantly influence the catalyst activity and selectivity in methyl chloride synthesis. The reason that the precursor type did not influence the activity is that during the reaction the catalyst is chlorinated in situ by the reactant HCl.

Acknowledgements

This work is a part of the activities at the Åbo Akademi Process Chemistry Centre (PCC) within a Centre of Excellence financed by Åbo Akademi University. Economic support from the Academy of

Finland and the Graduate School of Chemical Engineering (GSCE) is gratefully acknowledged.

The authors are grateful to Xuan Liu for the zeta potential measurements.

References

[1] K. Weissermel, H.-J. Arpe, Industrial Organic Chemistry, Wiley-VCH Verlag GmbH & Co. KGaA, Weinheim, 2003.
[2] M.T. Holbrook, Ethyl Chloride, Kirk-Othmer Encyclopedia of Chemical Technology, vol. 16, 5th ed., John Wiley & Sons, Inc., 2003.
[3] S.A. Schmidt, N. Kumar, A. Shukarev, K. Eränen, J.-P. Mikkola, D.Y. Murzin, T. Salmi, Appl. Catal. A 468 (2013) 120–134.
[4] E.B. Svetlanov, R.M. Flid, R.V. Dzhagatspanyan, A.M. Taber, Zhurnal Fizicheskoi Khimii 41 (1967) 920–921.
[5] T.M. Tovar, M. Stewart, S.L. Scott, Top. Catal. 55 (2012) 530–537.
[6] S.K. Pillai, S. Hamoudi, K. Belkacemi, Fuel 110 (2013) 32–39.
[7] S.K. Pillai, S. Hamoudi, K. Belkacemi, Appl. Catal. A 455 (2013) 155–163.
[8] M. Conte, T. Davies, A.F. Carley, A.A. Herzing, C.J. Kiely, G.J. Hutchings, J. Catal. 252 (2007) 23–29.
[9] C.A. Emeis, J. Catal. 141 (1993) 347–354.
[10] L. Zhang, C.M.B. Holt, E.J. Luber, B.C. Olsen, H. Wang, M. Danaie, X. Cui, X. Tan, V. Lui, W.P. Kalisvaart, D. Mitlin, J. Phys. Chem. C 115 (2011) 24381–24393.
[11] V. Meille, S. Pallier, P. Rodriguez, Colloids Surf. A 336 (2009) 104–109.
[12] G.V. Franks, Y. Ganz, J. Am. Ceram. Soc. 90 (2007) 3373–3388.
[13] C. Morterra, G. Magnacca, Catal. Today 27 (1996) 497–532.
[14] M. Digne, P. Sautet, P. Raybaud, P. Euzen, H. Toulhoat, J. Catal. 226 (2004) 54–68.
[15] H. Knözinger, P. Ratnasamy, Catal. Rev. Sci. Eng. 17 (1) (1978) 31–70.
[16] D.T. Lundie, A.R. McInroy, R. Marshall, J.M. Winfield, P. Jones, C.C. Dudman, S.F. Parker, C. Mitchell, D. Lennon, J. Phys. Chem. B 109 (2005) 11592–11601.
[17] I. Nastova, T. Skapin, L. Pejov, Surf. Sci. 605 (2011) 1525–1536.
[18] X. Liu, R.E. Truitt, J. Am. Chem. Soc. 119 (1997) 9856–9860.
[19] G. Busca, Catal. Today 226 (2014) 2–13.
[20] N.S. Gill, R.H. Nuttall, D.E. Scaife, D.A. Sharp, J. Inorg. Nucl. Chem. 18 (1961) 79–87.
[21] R. Wischert, P. Laurent a, C. Copéret, F. Delbecq, P. Sautet, J. Am. Chem. Soc. 134 (2012) 14430–14449.
[22] G. Busca, V. Lorenzelli, G.R. Amis, R.J. Willey, Langmuir 9 (1993) 1491–1499.
[23] S. Peulon, D. Lincot, Adv. Mater. 8 (1996) 166–170.
[24] L. Smrcok, V. Langer, J. Krestan, Acta Crystalallogr. C 62 (2006) pi83–pi84.
[25] J.C. Waerenborgh, M.O. Figueiredo, J.M.P. Cabral, L.C.J. Pereira, J. Solid State Chem. 111 (1994) 300–309.
[26] S. Arndt, B. Uysal, A. Berthold, T. Otrebma1, Y. Aksu, M. Driess, R. Schomäcker, J. Nat. Gas Chem. 21 (2012) 581–594.
[27] S.A. Schmidt, N. Kumar, A. Reinsdorf, K. Eränen, J. Wärnå, D.Y. Murzin, T. Salmi, Chem. Eng. Sci. 95 (2013) 232–245.
[28] P. Mäki-Arvela, D.Y. Murzin, Appl. Catal. A 451 (2013) 251–281.
[29] J. Kiennemann, C. Pagnoux, T. Chartier, J.F. Baumard, J.M. Lamerant, J. Am. Ceram. Soc. 12 (2004) 2175–2182.
[30] E. Laiti, P. Persson, L.-O. Öhman, Langmuir 14 (1998) 825–831.
[31] G. Lefèvre, M. Duc, P. Lepeut, R. Caplain, M. Fédoroff, Langmuir 18 (2002) 7530–7537.
[32] T. Rabung, T. Stumpf, H. Geckeis, R. Klenze, J.I. Kim, Radiochim. Acta 88 (2000) 711–716.
[33] S. Alami-Younssi, A. Larbot, M. Persin, J. Sarrazin, L. Cot, J. Membr. Sci. 91 (1994) 87–95.
[34] S. Peulon, D. Lincot, J. Electrochem. Soc. 145 (1998) 864–874.
[35] G.E. Maciel, L. Simeral, J.J.H. Ackerman, J. Phys. Chem. 81 (1977) 263–267.
[36] A. Zirino, S. Yamamoto, Limnol. Oceanogr. 17 (1972) 661–671.
[37] H.B. Silber, D. Simon, F. Gaizer, Inorg. Chem. 23 (23) (1984) 2844–2848.
[38] X.G. Zhang, Corrosion and Electrochemistry of Zinc, Springer, 1996.
[39] M. Digne, P. Sautet, P. Raybaud, P. Euzen, H. Toulhoat, J. Catal. 211 (2002) 1–5.
[40] A.A. Tsyganenko, V.N. Filimonov, J. Mol. Struct. 19 (1973) 579–589.
[41] S.A. Schmidt, N. Kumar, B. Zhang, K. Eränen, D.Y. Murzin, T. Salmi, Ind. Eng. Chem. Res. 51 (2012) 4545–4555.